

Equilibrium Sequences of Rotating Neutron Stars for New Realistic Equations of State

B. Datta¹ *, A. V. Thampam¹ and I. Bombaci²

¹ Indian Institute of Astrophysics, Bangalore 560 034, INDIA.

² Dipartimento di Fisica, Università di Pisa, and INFN Sezione di Pisa, Piazza Torricelli 2, I-56100 Pisa, ITALY

Abstract. For four newly suggested realistic equations of state of neutron star matter, we construct equilibrium sequences of rapidly rotating neutron stars in general relativity. The sequences are the normal and supramassive evolutionary sequences of constant rest mass. We find that for these equations of state the maximum (gravitational) mass rotating models occur (in central density and rotation rate Ω) before the maximum- Ω models. We calculate equilibrium sequences for a constant value of Ω corresponding to the most rapidly rotating pulsar PSR 1937+21. Also calculated is the radius of the marginally stable orbit and its dependence on Ω , relevant for modeling of kilo-Hertz quasi-periodic oscillations in X-ray binaries.

Key words: equation of state – pulsars: general – relativity – stars:neutron – stars: rotation

1. Introduction

Equilibrium sequences of rapidly rotating neutron stars are important in modelling a variety of phenomena of astrophysical interest, such as millisecond pulsars, low-mass X-ray binaries (LMXBs) and Quasi Periodic Oscillators (QPOs). Models of rapidly rotating neutron stars in general relativity must be constructed numerically. Early work on this have been based on incompressible fluids and polytropic models (Bonazzola & Schneider 1974; Butterworth 1976). In 1986 Friedman et al. (1986) reported calculations of rapidly rotating neutron stars in general relativity using a set of realistic equations of state (EOS) for neutron star matter. A similar work based on a formalism due to Komatsu et al. (1989) (KEH formalism) was done by Cook et al. (1994) for purpose of studying quasi-stationary evolution of isolated neutron stars. An alternative approach based on spectral methods was developed by Bonazzola et al. (1993). Extensive calculations using the spectral method for a broad set of realistic EOS of neutron star matter were presented in Salgado et al. (1994a; 1994b).

A key input in determining the structure of neutron stars is the EOS of high density matter. The work of Friedman et al. (1986) and that of Cook et al. (1994) make abundantly clear that the EOS also plays a significant role in deciding the various

equilibrium sequences of rotating neutron stars. For example, the Keplerian frequency of a test particle in orbit around a neutron star ranges from 55% of its spherical value for models based on the softest EOS to 75% of the spherical value for models with the stiffest EOS. The spreads in rotation-induced changes in the values of masses and radii from static neutron star cases also display considerable EOS dependence. These quantities (especially the Keplerian frequency of a particle in orbit around the rotating neutron star and the radius of the innermost stable circular orbit) are important for deciding the boundary layer structure and hence the emission characteristic of LMXB and QPOs.

Although dense matter has been a subject of study for nearly three decades now, there is no general agreement still on its exact composition, and on its EOS, especially for densities in excess several times nuclear matter density. The bulk of a neutron star (*core*) is made up of an electrically neutral quantum fluid composed of neutrons, protons, electrons and muons in equilibrium with respect to the weak interactions (beta-stable nuclear matter). However, at ultra-high densities, a variety of new and exotic hadronic degrees of freedom may become important (like hyperons, a K^- condensate or a deconfined phase of quark matter). The possible appearance of such an exotic core has enormous consequences for the transport properties of neutron stars and also for the formation of black holes (Brown & Bethe 1994; Bombaci 1996). The consequences of the existence of an exotic core (such as quark matter or kaon condensation) on the properties of rapidly rotating neutron stars will be reported in a forthcoming paper (Datta et al. 1997). In the present work, we have considered a conventional picture assuming the neutron star core to be composed of only beta-stable nuclear matter. Even in this picture, the determination of the EOS of asymmetric nuclear matter to describe the core of the neutron star, remains a formidable theoretical problem. In fact, one has to extrapolate the EOS to extreme conditions of high density and high neutron-proton asymmetry, *i.e.* in a regime where the EOS is poorly constrained by nuclear data and experiments. Astrophysical observational data, such as based on the binary pulsar PSR 1913+16, which give $1.4 M_\odot$ as the mass of the neutron star in the binary (Taylor & Weisberg 1989) and analysis of Vela pulsar postglitch timing data can be used to broadly rule out very soft EOS (Datta & Alpar 1993). Recently, some new EOS of asymmetric nuclear matter have been calculated and applied to the study of

*Also at Raman Research Institute, Bangalore 560 080, INDIA

non-rotating neutron stars (Baldo et al. 1997, Bombaci 1995). These EOS are based on (i) a microscopic Brueckner–Bethe–Goldstone many–body approach and (ii) a phenomenological model based on effective nuclear forces. These satisfy the basic requirements of reproducing the empirical saturation point for symmetric nuclear matter, the symmetry energy and the incompressibility parameter at the saturation density (see Table 1). These models have the desirable physical feature that the velocity of sound in the medium does not violate the causality condition. Therefore, these can be taken to be *realistic* EOS, and so it would be of interest to see the equilibrium rotating sequences that would be possible with these EOS. In this paper we report calculations of equilibrium sequences of rapidly rotating neutron stars in general relativity for these new realistic EOS models. The various equilibrium sequences that we construct are normal and supramassive evolutionary sequences of constant rest mass. In addition, we build equilibrium sequences for a constant value of rotation rate corresponding to a period of $P = 1.558$ ms of the millisecond pulsar PSR 1937+21 (Backer et al. 1982), the most rapidly rotating pulsar known.

2. Rapidly and Rigidly Rotating Relativistic Stars

The space–time around a rotating neutron star can be described in quasi–isotropic coordinates, as a generalization of Bardeen’s metric (Bardeen 1970):

$$\begin{aligned} ds^2 &= g_{\mu\nu}dx^\mu dx^\nu (\mu, \nu = 0, 1, 2, 3) \\ &= -e^{\gamma+\rho}dt^2 + e^{2\alpha}(r^2d\theta^2 + dr^2) + e^{\gamma-\rho}r^2\sin^2\theta \\ &\quad (d\phi - \omega dt)^2 \end{aligned} \quad (1)$$

where $g_{\mu\nu}$ is the metric tensor. The metric potentials γ , ρ , α , and the angular velocity of the stellar fluid relative to the local inertial frame (ω) are all functions of the quasi–isotropic radial coordinate (r) and the polar angle (θ). We use here geometric units: $c = 1 = G$. We assume a perfect fluid description, for which the energy momentum tensor is given by:

$$T^{\mu\nu} = (\epsilon + P)u^\mu u^\nu + Pg^{\mu\nu} \quad (2)$$

where ϵ is the total energy density, P the pressure and u^μ the unit time–like four velocity vector that satisfies

$$u^\mu u_\mu = -1 \quad (3)$$

The proper velocity v of the matter, relative to the local Zero Angular Momentum Observer (ZAMO), is given in terms of the the angular velocity $\Omega \equiv u^3/u^0$ of the fluid element (measured by a distant observer in an asymptotically flat space–time), by the following equation (see Bardeen 1970):

$$v = (\Omega - \omega)rs\sin\theta e^{-\rho} \quad (4)$$

The four velocity (u^μ) of the matter can be written as

$$u^\mu = \frac{e^{-(\gamma+\rho)/2}}{(1-v^2)^{1/2}}(1, 0, 0, \Omega) \quad (5)$$

Substitution of the above into Einstein field equations projected on to the frame of reference of a ZAMO yield three elliptic equations for the metric potentials ρ , γ and ω and two linear ordinary differential equations for the metric potential α (Komatsu et al. 1989; Butterworth & Ipser 1976; Bardeen & Wagoner 1971). In the KEH formalism (Komatsu et al. 1989), the elliptic differential equations are converted to integral equations for the metric potentials using Green’s function approach.

From the relativistic equations of motion, the equation of hydrostatic equilibrium for a barytropic fluid may be obtained as:

$$h(P) - h_p \equiv \int_{P_p}^P \frac{dP}{(\epsilon + P)} = \ln u^t - \ln u_p^t - \int_{\Omega_c}^{\Omega} F(\Omega) d\Omega \quad (6)$$

where $h(P)$ is termed as the specific enthalpy. P_p , u^t are the rescaled values of pressure and t-component of the four velocity respectively and h_p is the specific enthalpy at the pole; $F(\Omega) = u^t u_\phi$ is the integrability condition imposed on the equation of hydrostatic equilibrium, and it can be physically interpreted as the rotation law for the matter constituting the neutron star. An appropriately chosen value of h_p defines the surface of the star. Equation (6) shows that the hydrostatic equilibrium equation is integrable if $P(\epsilon)$ and $u^t u_\phi$ are specified.

As shown by Bardeen 1970 (see also Butterworth & Ipser 1976), the quantity $u^t u_\phi$ is a function of Ω only. Komatsu et al. (1989) have suggested the following specific form for $F(\Omega)$:

$$F(\Omega) = A^2(\Omega_c - \Omega) \quad (7)$$

where A is a rotation constant such that when $A \rightarrow \infty$, the configuration approaches rigid rotation (that is, $\Omega = \Omega_c$) so that $F(\Omega)$ is finite. Furthermore, when $A \rightarrow 0$, the configuration should approach that of rotation with constant specific angular momentum.

On substituting Eqs. (5) and (7) into Eq. (8), we have the hydrostatic equilibrium equation as

$$\begin{aligned} h(P) - h_p &= \frac{1}{2}[\gamma_p + \rho_p - \gamma - \rho - \ln(1 - v^2) + \\ &\quad A^2(\Omega - \Omega_c)^2] \end{aligned} \quad (8)$$

where γ_p and ρ_p are the values of the metric potentials at the pole, and $\Omega = r_e \Omega$.

Therefore, the hydrostatic equilibrium equations at the centre and equator for a rigidly rotating neutron star become respectively

$$h(P_c) - h_p - \frac{1}{2}[\gamma_p + \rho_p - \gamma_c - \rho_c] = 0 \quad (9)$$

$$(\gamma_p + \rho_p - \gamma_e - \rho_e) - \ln[1 - (\Omega_e - \omega_e)^2 r_e^2 e^{-2\rho_e}] = 0 \quad (10)$$

where the subscripts p, e and c on the variables stand respectively for the corresponding values at the pole, equator and center.

We solve (numerically) the integral equations for ρ , γ and ω , the ordinary differential equation (in θ) for the metric potential α , together with Eqs. (8), (9) and (10), iteratively to obtain ρ , γ , α , ω , the equatorial coordinate radius (r_e), angular velocity (Ω), and the density (ϵ) and pressure (P) profiles.

2.1. Innermost stable orbits

Since the metric (1) is stationary and axisymmetric, the energy and angular momentum are constants of motion. Therefore, for a particle in stable orbit around the neutron star, the specific energy E (in units of the rest energy $m_0 c^2$, where m_0 is the rest mass of the particle) and the specific angular momentum l (in units of $m_0 c$) can be identified as $-p_0$ and p_3 respectively, where, p_μ ($\mu = 0, 1, 2, 3$), stands for the four-momentum of the particle. From the condition $p_\mu p^\mu = -1$, we have the equations of motion of the particle (confined to the equatorial plane) in this gravitational field as

$$\dot{t} = \frac{dt}{d\tau} = p^0 = e^{-(\gamma+\rho)}(E - \omega l) \quad (11)$$

$$\dot{\phi} = \frac{d\phi}{d\tau} = p^3 = \Omega p^0 = e^{-(\gamma+\rho)}\omega(E - \omega l) + \frac{l}{r^2 e^{(\gamma-\rho)}} \quad (12)$$

$$r^2 \equiv e^{2\alpha+\gamma+\rho} \left(\frac{dr}{d\tau} \right)^2 = E^2 - V^2. \quad (13)$$

Here, τ is the proper time and V is the effective potential given by

$$V^2 = e^{\gamma+\rho} \left[1 + \frac{l^2/r^2}{e^{\gamma-\rho}} \right] + 2\omega El - \omega^2 l^2. \quad (14)$$

The conditions for circular orbits, extremum of energy and minimum of energy are respectively:

$$E^2 = V^2 \quad (15)$$

$$V_{,r} = 0 \quad (16)$$

$$V_{,rr} > 0. \quad (17)$$

For marginally stable orbits,

$$V_{,rr} = 0. \quad (18)$$

In our notation, a comma followed by one 'r' represents a first order partial derivative with respect to r , etc..

From the expression for the effective potential and the conditions (15), (16) and (17), one obtains three equations in the three unknowns: namely, r , E , and l . In principle, if analytical expressions for $e^{\gamma+\rho}$, $e^{2\alpha}$, $e^{\gamma-\rho}$ and ω are known, it would be a straightforward exercise to solve these equations to obtain r , E , and l . In practice, however, this is not so, and the solutions for the metric coefficients $e^{\gamma+\rho}$, $e^{2\alpha}$, $e^{\gamma-\rho}$, and ω have to be obtained as arrays of numbers for various values of r and θ using a numerical method. Furthermore, the condition (18) will introduce second order derivatives of γ , ρ , and ω , which means that care has to be exercised in ensuring the numerical accuracies of the quantities calculated. For this purpose, it is convenient to express E and l in terms of the physical velocity v using Eq. (4) (Bardeen 1972) as:

$$E - \omega l = \frac{e^{(\gamma+\rho)/2}}{\sqrt{1-v^2}} \quad (19)$$

$$l = \frac{v r e^{(\gamma-\rho)/2}}{\sqrt{1-v^2}}. \quad (20)$$

Eqs. (19) and (20) can be recognized as the condition for circular orbits. Conditions (16) and (18) yield respectively,

$$v = \pm \left(\sqrt{e^{-2\rho} r^4 \omega_{,r}^2 + 2r(\gamma_{,r} + \rho_{,r}) + r^2(\gamma_{,r}^2 - \rho_{,r}^2)} \pm e^{-\rho} r^2 \omega_{,r} \right) / (2 + r(\gamma_{,r} - \rho_{,r})) \quad (21)$$

$$V_{,rr} \equiv 2 \left[\frac{r}{4} (\rho_{,r}^2 - \gamma_{,r}^2) - \frac{1}{2} e^{-2\rho} \omega_{,r}^2 r^3 - \rho_{,r} + \frac{1}{r} \right] v^2 + [2 + r(\gamma_{,r} - \rho_{,r})] v v_{,r} - e^{-\rho} \omega_{,r} v v_{,r} + \frac{r}{2} (\gamma_{,r}^2 - \rho_{,r}^2) - e^{-\rho} r^2 \omega_{,r} v_{,r} = 0 \quad (22)$$

where we have made use of Eq. (21) and its derivative with respect to r in order to eliminate the second order derivatives in Eq. (22). The zero of $V_{,rr}$ will give the innermost stable circular orbit radius (r_{orb}). In Eq. (21), the positive sign refers to the co-rotating particles and the negative sign to the counter-rotating particles. In this study we have considered only the co-rotation case.

3. Numerical Procedure

The numerical procedure followed by us is the KEH formalism. This is based on an earlier work by Hachisu (1986) which has a self-consistency requirement that requires that the maximum (central) energy density ϵ_c and the ratio of the polar to equatorial radial coordinates r_p/r_e be fixed for each iterative cycle. If ρ^i , γ^i , α^i and r_e^i are the values of the corresponding parameters during the i^{th} iterative cycle, then:

1. these values are first scaled (divided) by $(r_e^i)^2$ to obtain $\hat{\rho}^i$, $\hat{\gamma}^i$ and $\hat{\alpha}^i$ respectively.
2. a new value of r_e is calculated using Eq. (10) for $\epsilon = \epsilon_c$ i.e. $v = 0$ so that

$$r_e^{i+1} = \frac{2[h(P(\epsilon_c)) - h_p]}{\hat{\gamma}_p^i + \hat{\rho}_p^i - \hat{\gamma}_c^i - \hat{\rho}_c^i} \quad (23)$$

3. the value of Ω_c is computed from Eq. (11) as

$$\Omega_c^{i+1} = \hat{\omega}_e^i + e^{\rho_e^i} \left[1 - e^{(\gamma_p^i + \rho_p^i - \gamma_e^i - \rho_e^i)} \right] \quad (24)$$

4. the values of the three scaled metric potentials $\hat{\rho}^i$, $\hat{\gamma}^i$ and $\hat{\alpha}^i$ are rescaled (multiplied) by $(r_e^{i+1})^2$
5. using these values of r_e^{i+1} , Ω_c^{i+1} , ρ^i , γ^i , α^i , $\hat{\omega}^i$, equation (9) is solved to obtain the matter energy distribution namely ϵ^{i+1} , P^{i+1} , v^{i+1} etc.
6. the integral equations for the metric potentials are solved to obtain ρ^{i+1} , γ^{i+1} , $\hat{\omega}^{i+1}$ and α^{i+1} .
7. steps (1) to (6) are repeated until r_e converges to within a tolerance of 10^{-5} .

Once r_e converges, the metric potentials ρ , γ , ω and α together with the density (ϵ) and pressure (P) profiles can be used to compute the structure parameters (see Cook et al. 1994).

4. New Equation of State Models

4.1. Microscopic equation of state

In a microscopic approach the input is the two-body nucleon-nucleon (NN) interaction, described by so-called *realistic* interactions like the Argonne, Bonn, Nijmegen, Paris, Urbana

potentials (see *e.g.* Machleidt 1989). The theoretical basis to construct these realistic NN potentials is the meson-exchange theory of nuclear forces. In this scheme, nucleons, nucleon resonances (*e.g.* $\Delta(1232)$), and mesons such as π , ρ and ω , are incorporated in a potential representation. The various parameters in the potential are then adjusted to reproduce the experimental data for the two-body problem (deuteron properties and NN scattering phase shifts). Then one has to solve the complicated many-body problem to get the EOS.

Recently, Baldo et al. (1997), hereafter BBB, have computed a new EOS of beta-stable nuclear matter, and with this EOS they have calculated the structure of non-rotating neutron stars. In their approach, the energy per nucleon of nuclear matter is obtained in the Brueckner-Hartree-Fock (BHF) approximation of the Brueckner-Bethe-Goldstone theory. The only input quantity for these calculations is the nuclear interaction. In their calculation BBB used the Argonne v14 (Av14) (Wiringa et al. 1984) or the Paris (Lacombe et al. 1980) two-body nuclear force, implemented in both cases by the Urbana three-body force (TBF) (Carlson et al. 1983; Schiavilla et al. 1986). As is well known, the need for a TBF arises to obtain a correct saturation point of symmetric nuclear matter in a non-relativistic many-body approach. In the following we refer to the EOS obtained in BBB with the Av14+TBF and Paris+TBF, as the BBB1 and BBB2 equation of state respectively. The saturation properties for these two microscopic models are summarized in Table 1, and the calculated speed of sound is shown in Fig. 1. The latter always remains within the causality bound.

4.2. Phenomenological equation of state

In this case the input is a density-dependent effective NN interaction. The most popular of this kind of interaction is the Skyrme interaction (Skyrme 1956). In the present work we used a generalized Skyrme-like EOS developed in ref. (Bombaci 1995), and we refer to it as the BPAL EOS. An important feature of the BPAL models is the possibility to have different forms for the density dependence of the potential part $E_{sym}^{pot}(n)$ of the nuclear symmetry energy, modelling different results predicted by microscopic calculations (Wiringa et al. 1988, Bombaci & Lombardo 1991). In particular, E_{sym}^{pot} is proportional to the nucleon number density n in the case of BPAL32, and to \sqrt{n} in the case of BPAL21 EOS. The density dependence of the symmetry energy plays a very important role in the physics of neutron stars. This function determines the proton fraction in beta-stable nuclear matter, which, in turn, is crucial for an accelerated rate of cooling of a neutron star through the so-called direct Urca process above a critical value of the proton fraction (Lattimer et al. 1991; Page & Applegate 1992).

In Fig. 2 we plot the pressure-density relationship for EOS models BBB1, BBB2, BPAL21 and BPAL32 (curves 1–4) and also compare it with two other EOS models, one of which is a *very soft* EOS BPAL12 (Bombaci 1995) and the other a *very stiff* EOS (Sahu et al. 1993):

(1) Soft: *BPAL21* (Bombaci 1995): This EOS is characterized by $K_0 = 120$ MeV and $E_{sym}^{pot} \sim n$. The value 120 MeV for the incompressibility is unrealistically small when compared with the value 220 ± 30 MeV extracted from nuclear phenomenology (Blaizot 1980; Myers & Swiatecky 1996), however BPAL12 EOS is still able to sustain the measured mass $1.44 M_\odot$ of the pulsar PSR1916+13 as the maximum grav-

tational mass of non-rotating neutron stars constructed with this EOS is $1.46 M_\odot$.

(2) Stiff: *Sahu et al. (1993)*: This is a field theoretical EOS for neutron matter in beta equilibrium based on the chiral sigma model. The model includes an isoscalar vector field generated dynamically and reproduces the empirical values of the nuclear matter saturation density and binding energy and also the isospin symmetry coefficient for asymmetric nuclear matter. The energy per nucleon of nuclear matter according to Sahu et al. (1993) is in very good agreement, up to about four times the equilibrium nuclear matter density, with estimates inferred from heavy-ion collision experimental data. The maximum gravitational mass of non-rotating neutron stars constructed with this EOS is $2.59 M_\odot$.

For our computations, we constructed the composite EOS for the entire span of neutron star densities by joining the new high density EOS models to that of Negele & Vautherin (1973) for the density range $(10^{14} - 5 \times 10^{10}) g cm^{-3}$, Baym et al. (1972) for densities down to $\sim 10^3 g cm^{-3}$ and Feynman et al. (1949) for densities less than $10^3 g cm^{-3}$.

5. Results and Discussion

The equilibrium sequences of rotating neutron stars depend on two parameters: the central density (ϵ_c) and the rotation rate (Ω). For purpose of illustration, we choose three limits in this parameter space. These are: (i) the static or non-rotating limit, (ii) the limit at which instability to quasi-radial mode sets in and (iii) the centrifugal mass shed limit. The last limit corresponds to the maximum Ω for which centrifugal forces are able to balance the inward gravitational force.

Table 2 summarizes the non-rotating neutron star structure parameters for the EOS models BBB1, BBB2, BPAL21 and BPAL32. The values listed correspond to the maximum stable mass configuration. The entries in this table are the central density (ϵ_c), the gravitational mass (M_G), the rest (baryonic) mass (M_0) of the neutron star and the radius (R). The maximum mass is an indicator of the softness/stiffness of the EOS and its values as listed in Table 2 reflect that the EOS models used are all intermediate in stiffness. Among these, BPAL21 is the softest EOS and BPAL32 the stiffest one.

In Table 3 we list the following quantities corresponding to the maximum gravitational mass configurations: central density, rotation rate, moment of inertia (I), gravitational mass, ratio of rotational kinetic energy to total gravitational energy (T/W), equatorial radius, eccentricity (e) where e is defined to be $\sqrt{1 - R_p^2/R^2}$, R_p being the polar radius of the configuration, ratio of rotation rate (ω_c) of stellar fluid relative to the inertial frame at the centre of the star to the rotation rate, the angular momentum (J), the value of the radius of the innermost stable orbit (r_{orb}), the polar, forward and backward redshifts (Z_p, Z_f, Z_b), the rest mass (M_0) and the proper mass (M_p) of the neutron star. The values of these quantities are listed in Table 4 for the maximum angular momentum models. From Table 3, it can be seen that the gravitational mass of the maximum stable rotating configuration has a value that is close to $2 M_\odot$. Interestingly, this is close to predictions from analysis of LMXB observational data (Zhang et al. 1996). Therefore, if the internal constitution of the compact star in LMXBs were to be described by the EOS models that we have considered here, and furthermore, if it were to have a mass $\sim 2 M_\odot$, the star has to be rotating near centrifugal break-up speeds (rotation

periods ~ 0.5 ms). Interestingly, for such configurations, it can be seen from Table 3, that the separation of the innermost stable orbit from the neutron star surface (namely, the boundary layer extent) is highly EOS dependent. This separation ranges from 0.07 km to 1.031 km. This relatively large spread can be understood in terms of the spreads on values of ϵ_c and Ω corresponding to the centrifugal mass shed. These results will have relevance in modeling LMXBs/QPOs. For such neutron stars as the central objects in LMXBs, there will be a very significant re-ordering of the contributions of the disk and the boundary layer luminosities to the total luminosity (Thampan & Datta 1997).

The results of our computations for rotating neutron stars corresponding to the four new EOS models are given below.

5.1. EOS Model BPAL21

The normal sequences for this EOS have rest mass $M_0/M_\odot < 1.9395$ and supramassive sequences have rest mass $1.9395 < M_0/M_\odot < 2.2515$.

5.2. EOS Model BBB1

In Fig. 3 we show the functional dependence of the gravitational mass with central density. In this and all subsequent figures, the bold solid curve represents the non-rotating or static limit, and the bold dashed curve the centrifugal mass shed limit. The long dashed curve is the constant- Ω sequence corresponding to the period $P = 1.558$ ms. The thin solid curves that are roughly horizontal are the constant rest mass evolutionary sequences. The evolutionary sequences above the maximum stable non-rotating mass configuration are the supramassive evolutionary sequences, and those that are below this limit are the normal evolutionary sequences. The almost vertical thin dashed line is the limit for instability against quasi-radial modes. The supramassive evolutionary sequences beyond the quasi-radial mode instability limit are represented by dotted lines. The maximum mass sequence for this EOS corresponds to a rest mass value of $2.471 M_\odot$. The supramassive sequences lie in the rest mass range of $2.356 M_\odot < M_0 < 2.471 M_\odot$. The gravitational mass of the maximum stable rotating configuration is $2.135 M_\odot$ and its radius is 13.129 km. If we assume that the fastest pulsar known to date, PSR 1937+21, has the canonical mass value of $1.4 M_\odot$ and is described by EOS model BPAL21, then this neutron star should have a central density of about $1.2 \times 10^{15} g cm^{-3}$.

In Fig. 4 we give a plot of M_G as a function of R . For the millisecond pulsar PSR 1937 + 21 with an assumed mass value of $1.4 M_\odot$, this corresponds to a radius of 11 km.

In Fig. 5 we display the plot of Ω as a function of the specific angular momentum cJ/GM_0^2 . The inset shows a close-up view of the region surrounding the instability limit to quasi-radial mode near the centrifugal mass shed limit. It is clear from this figure that the maximum mass rotating model (represented by the plus sign) has a lower angular velocity than the maximum- Ω model (represented by the intersection of the line representing the instability to quasi-radial modes with that of the centrifugal mass shed limit).

5.3. EOS Model BBB2

The equilibrium sequences for BBB2 are displayed on Figs. 6 – 8 for the same representative set of parameters as for EOS model BBB1

For this EOS, the supramassive sequences have rest masses between $2.261 M_\odot$ and $2.653 M_\odot$ and the maximum mass at mass shed limit is $2.272 M_\odot$ with an equatorial radius of 12.519 km.

5.4. EOS Model BPAL32

This EOS model being the stiffest out of the four models that we consider here, has the highest value for the maximum rotating gravitational mass ($2.3 M_\odot$). The rest masses of supramassive sequences lie in the range $2.263 M_\odot < M_0 < 2.655 M_\odot$.

Since the behaviour of M with ϵ_c and R and that of Ω with cJ/GM_0^2 for EOS models BPAL21 and BPAL32 are more or less similar to those for EOS models BBB1 and BBB2, we do not display the corresponding figures for the former EOS models here.

In Table 5 we list the values of the various parameters for the constant Ω sequences for the four EOS models considered in this work. In general, r_{orb} exhibits three characteristics: (a) r_{orb} is non-existent (b) $r_{orb} < R$, and (c) $r_{orb} > R$. For the first two cases, r_{orb} is taken to be the Keplerian orbit radius at the surface of the star. From Table 5 it can be seen that for low central densities, stable orbits can exist all the way up to the surface of the neutron star but for high enough central densities, the boundary layer (the separation between the surface of the neutron star and its innermost stable orbit) can be substantial (~ 5 km for the maximum value of the listed central densities). These results will have applications in modeling accretion flows in LMXBs.

We now make a brief reference to other similar work. For equilibrium Keplerian angular velocity corresponding to the period of millisecond pulsar PSR 1937+21 and an assumed mass of $1.4 M_\odot$ for the neutron star, Friedman et al. (1986) suggest that stiff EOS for neutron star interior are favoured. A similar conclusion but based on a pulsar glitch model and the crustal moment of inertia considerations has been reported by Datta & Alpar (1993). The work of Friedman et al. (1986) show that for a given EOS, the models with maximum gravitational mass also have the greatest frequency of rotation. Cook et al. (1994) found that while models with maximum gravitational mass also (due to stability conditions defined by Friedman et al. 1988) have the maximum rotation rate Ω , the models for maximum gravitational mass and maximum- Ω do not in general coincide. In particular, for EOS models that display causality violation near or before the maximum stable mass non-rotating configuration, the maximum- Ω model occurs before (in central density and Ω) the maximum mass model at the mass shed limit. The EOS models that we have considered here do not violate the causality condition until well beyond the maximum stable mass non-rotating configuration. Our computations show that the maximum gravitational mass rotating models for these EOS occur (in central density and Ω) before the maximum- Ω models. In view of absence of correlation between QPO frequency and source count rate (as suggested by recent observations, see Berger et al. 1996; Zhang et al 1996), our results on marginally stable Keplerian orbits corresponding to realistic EOS will have application in

understanding kilo-Hertz quasi-periodic oscillations in X-ray binaries in terms of strong-field general relativity, where rapid rotation of the accreting neutron star is important.

Zhang W., Lapidus I., White N. E., Titarchuk L., 1996, ApJ 469, L17

References

Backer D. C., Kulkarni S. R., Heiles C., Davis M. M., Goss W. M., 1982, Nat 300, 615

Baldovin-Sotelo P., Bombaci I., Burgio G. F., 1997, A&A 328, 274, (BBB)

Bardeen J. M., 1970, ApJ 162, 71

Bardeen J. M., 1972, ApJ 178, 347

Bardeen J. M., Wagoner R. V., 1971, ApJ 167, 359

Baym G., Pethick C. J., Sutherland P. G., 1972, ApJ 170, 299

Berger M., van der Klis M., van Paradijs J., et al., 1986, ApJ 469, L13

Blaizot J. P., 1980, Phys. Rep. 64, 171.

Bombaci I., 1995, Perspectives on Theoretical Nuclear Physics. In: Bombaci I., Bonaccorso A., Fabrocini A., et al. (eds.) Proc. VI Convegno su Problemi di Fisica Nucleare Teorica, ETS, Pisa, p.223

Bombaci I., 1996, A&A 305, 871

Bombaci I., Lombardo U., 1991, Phys. Rev. C44, 1892

Bonazzola S., Schneider J., 1974, ApJ 191, 273

Bonazzola S., Gourgoulhon E., Salgado M., Marck J. A., 1993, A&A 278, 421

Brown G. E., Bethe H. A., 1994, ApJ 432, 659

Butterworth E. M., 1976, ApJ 204, 561

Butterworth E. M., Ipser J. R., 1976, ApJ 204, 200

Carlson J., Pandharipande V. R., Wiringa R. B., 1983, Nucl. Phys. A401, 59

Cook G. B., Shapiro S. L., Teukolsky S. A., 1994, ApJ 424, 823

Datta B., Alpar M. A., 1993, A&A 275, 210

Datta B., Thampan, A. V., Bombaci, I., 1997, in preparation

Friedman J. L., Ipser J. R., Parker L., 1986, ApJ 304, 115

Friedman J. L., Ipser J. R., Sorkin R. D., 1988, ApJ 325, 722

Feynman R. P., Metropolis N., Teller E., 1949, Phys. Rev. 75, 1561

Hachisu I., 1986, ApJS 61, 479

Komatsu H., Eriguchi Y., Hachisu I., 1989, MNRAS 237, 355

Lacombe M., Loiseau B., Richard J. M., et al., 1980, Phys. Rev. C21, 861

Lattimer J., Pethick C., Prakash M., Haensel P., 1991, Phys. Rev. Lett. 66, 2701

Machleidt R., 1989, Adv. Nucl. Phys. 19, 189

Myers W. D., Swiatecky W. J., 1996, Nucl. Phys. A601, 141.

Negele J. W., Vautherin D., 1973, Nucl. Phys. A207, 298

Page D., Applegate J.H., 1992, ApJ 394, L17

Sahu P. K., Basu R., Datta B., 1993, ApJ 416, 267

Salgado M., Bonazzola S., Gourgoulhon E., Haensel P., 1994a, A&A 291, 155

——— 1994b, A&AS 108, 455

Schiavilla R., Pandharipande V. R., Wiringa R. B., 1986, Nucl. Phys. A449, 219

Skyrme T. H. R., 1956, Philos. Mag. 1, 1043

Taylor J. H., Weisberg J. M., 1989, ApJ 345, 434

Thampan A. V., Datta B., 1998, MNRAS (in press)

Wiringa R. B., Smith R. A., Ainsworth T. L., 1984, Phys. Rev. C29, 1207

Wiringa R. B., Fiks V., Fabrocini A., 1988, Phys. Rev. C38, 1010

Fig 1

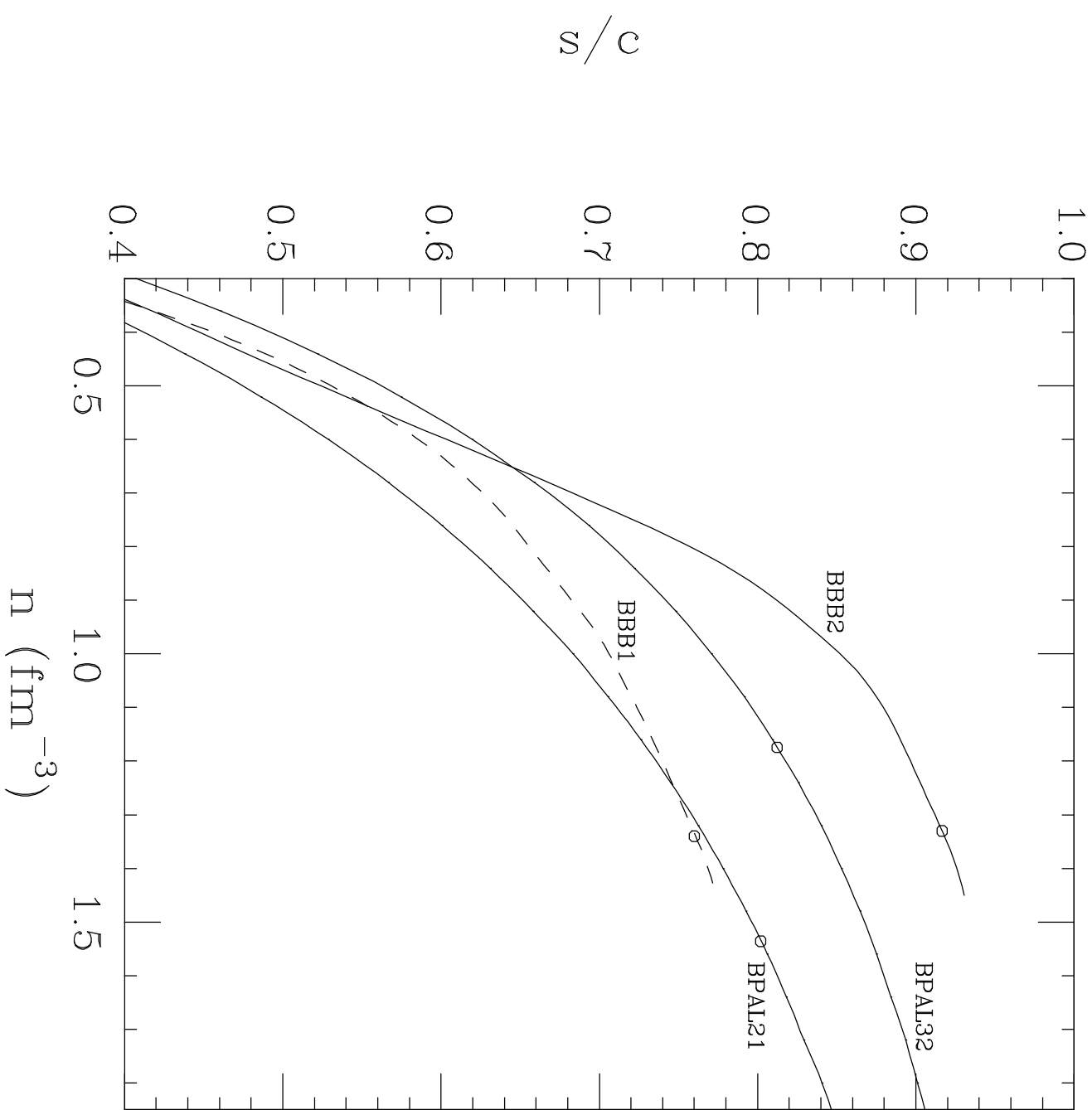


Fig 2

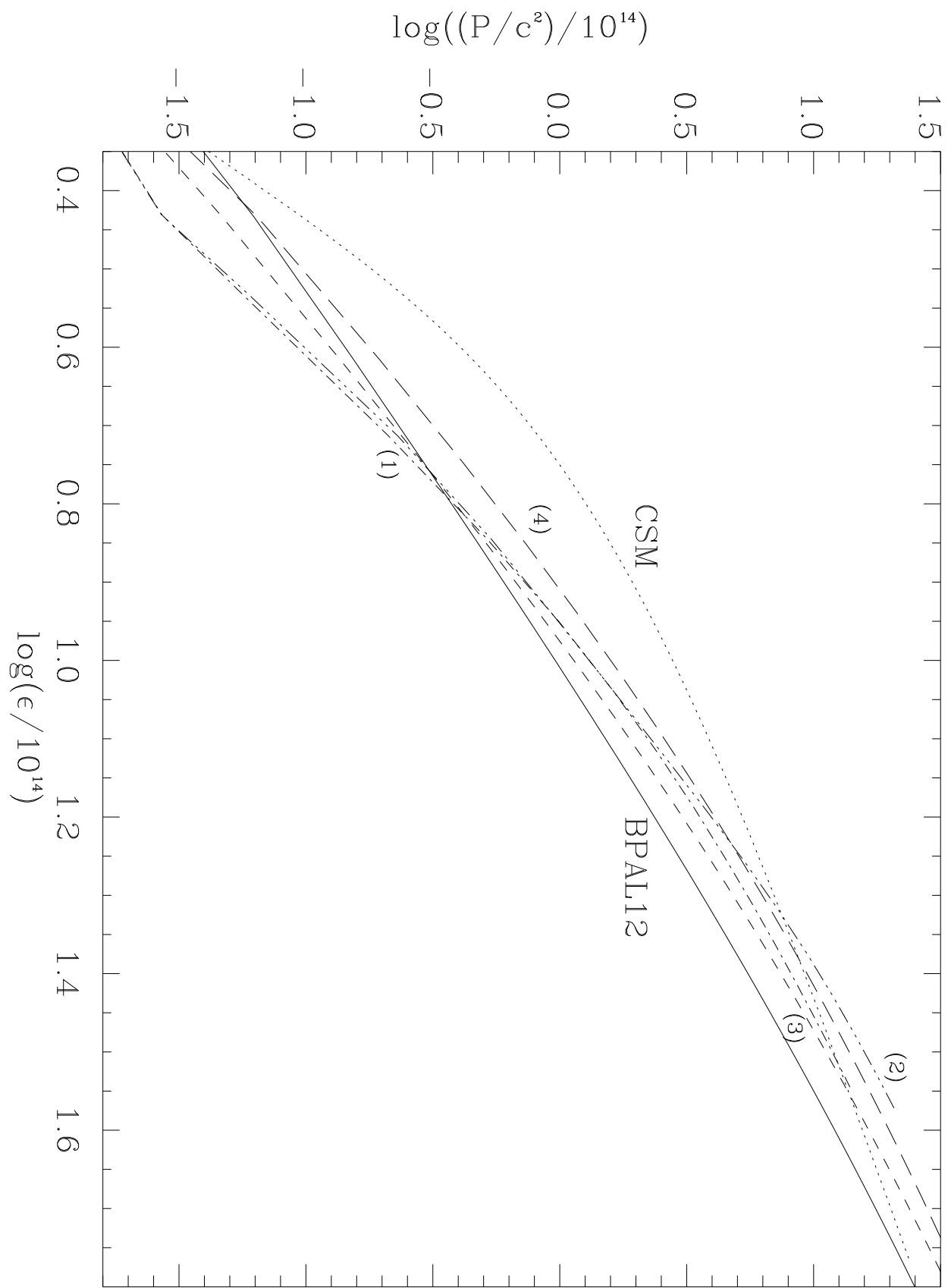


Fig 3

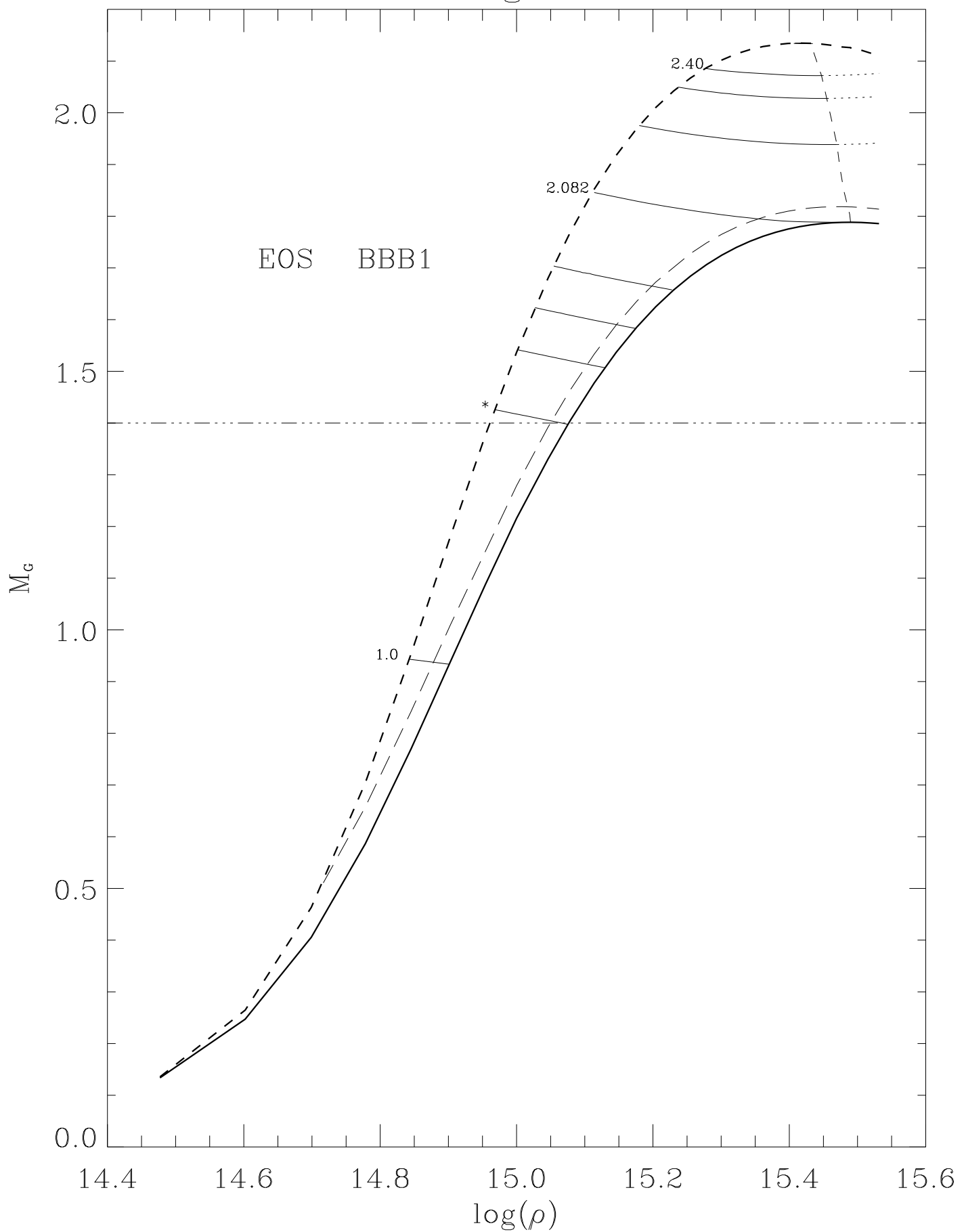


Fig 4

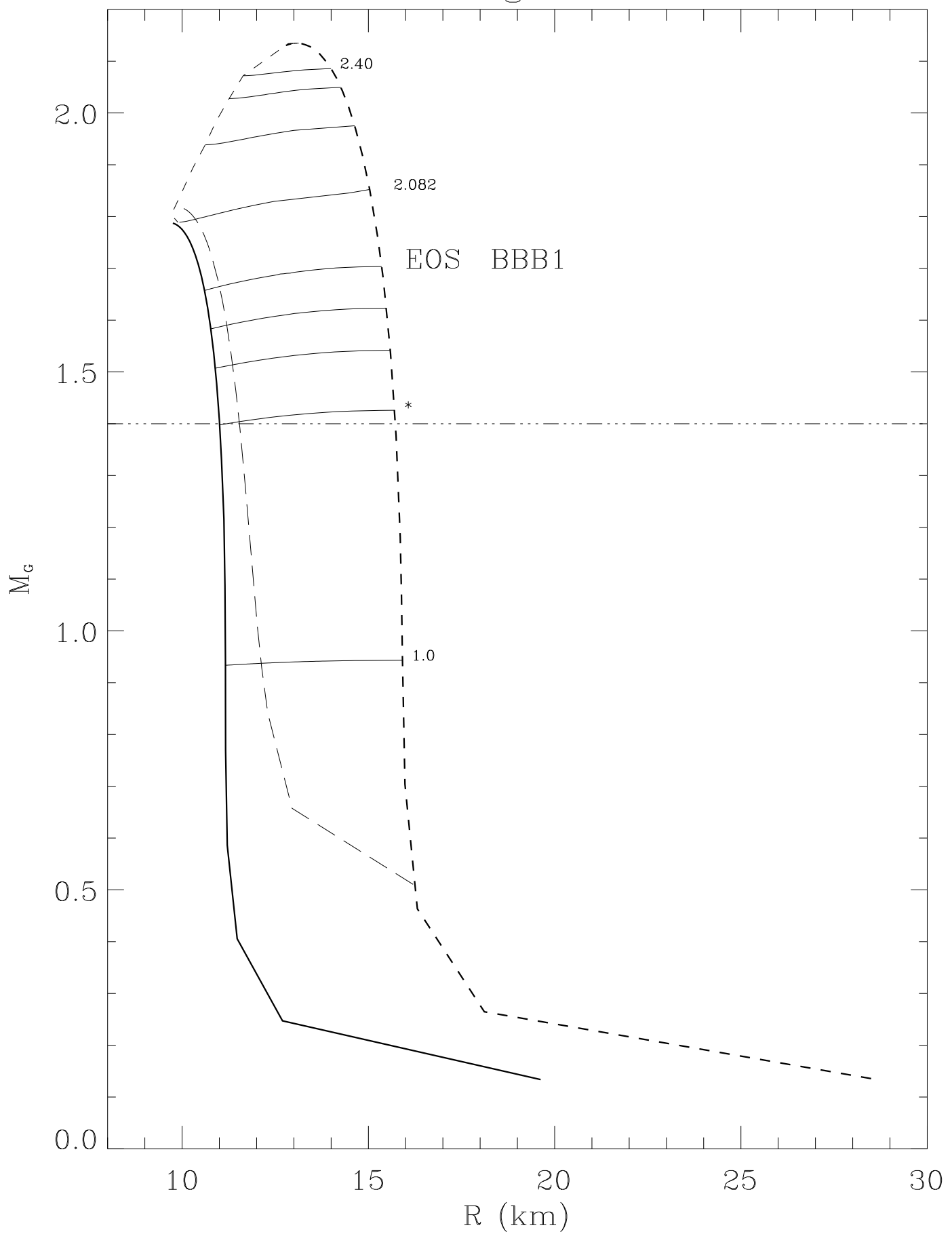


Fig 5

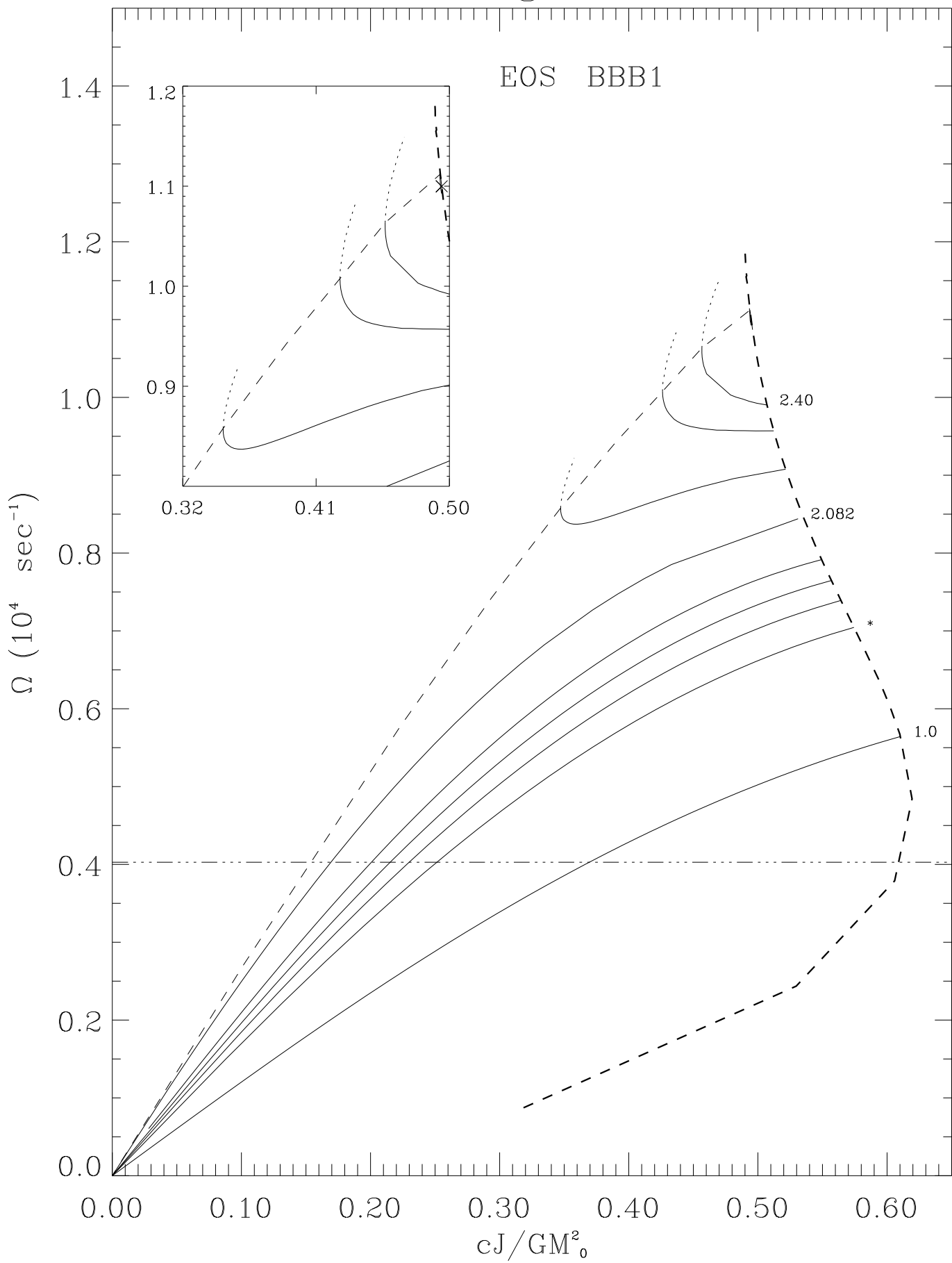


Fig 6

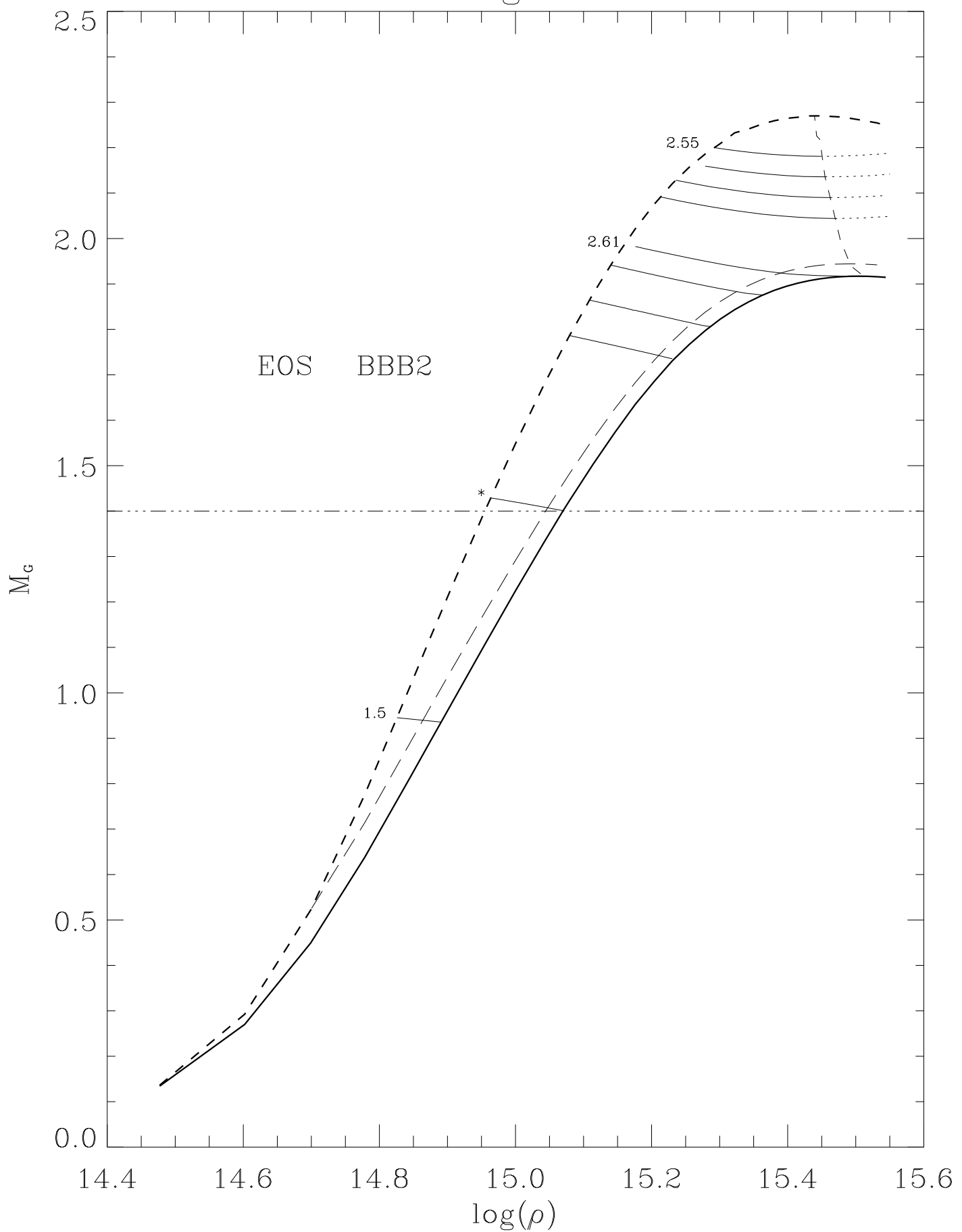


Fig 7

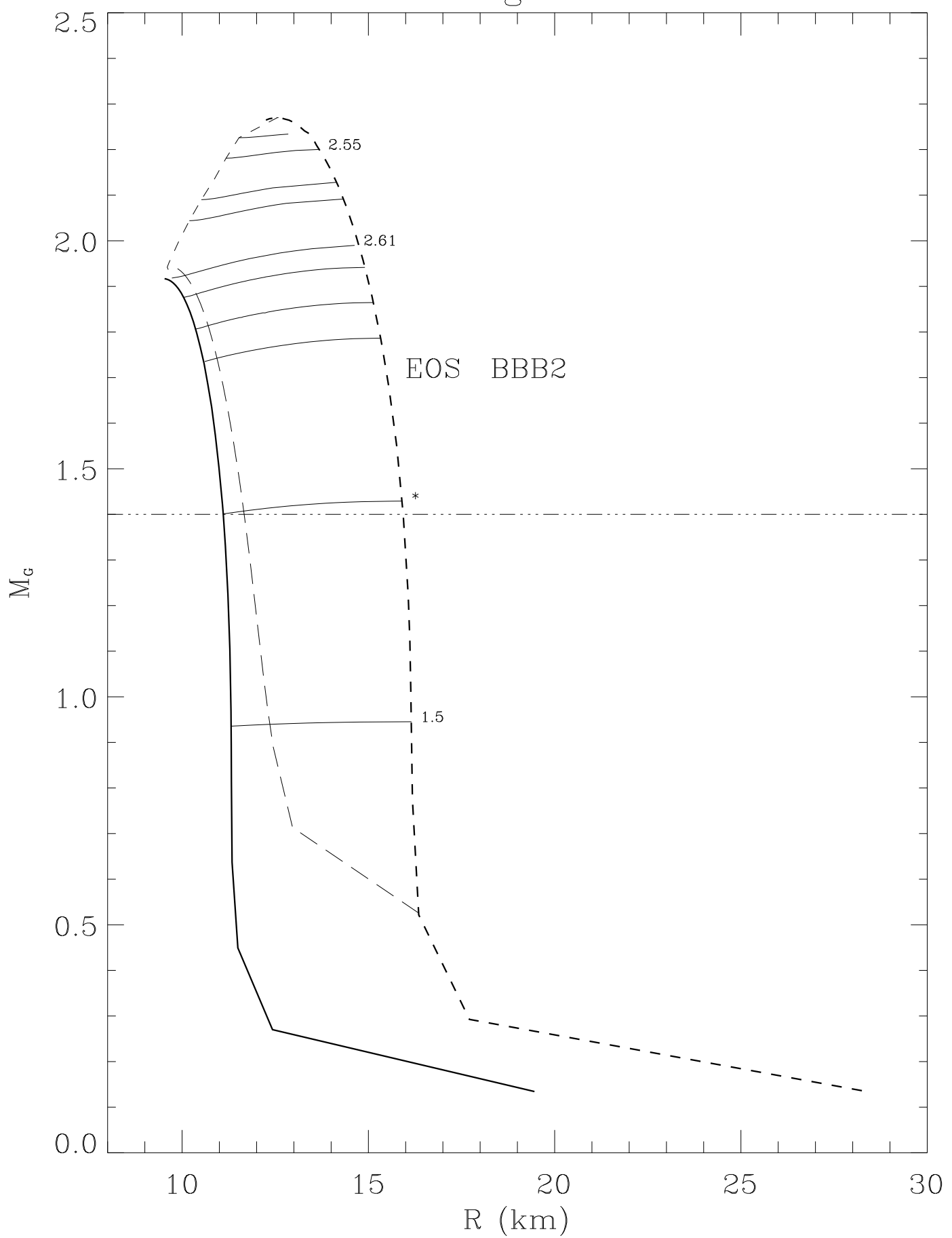


Fig 8

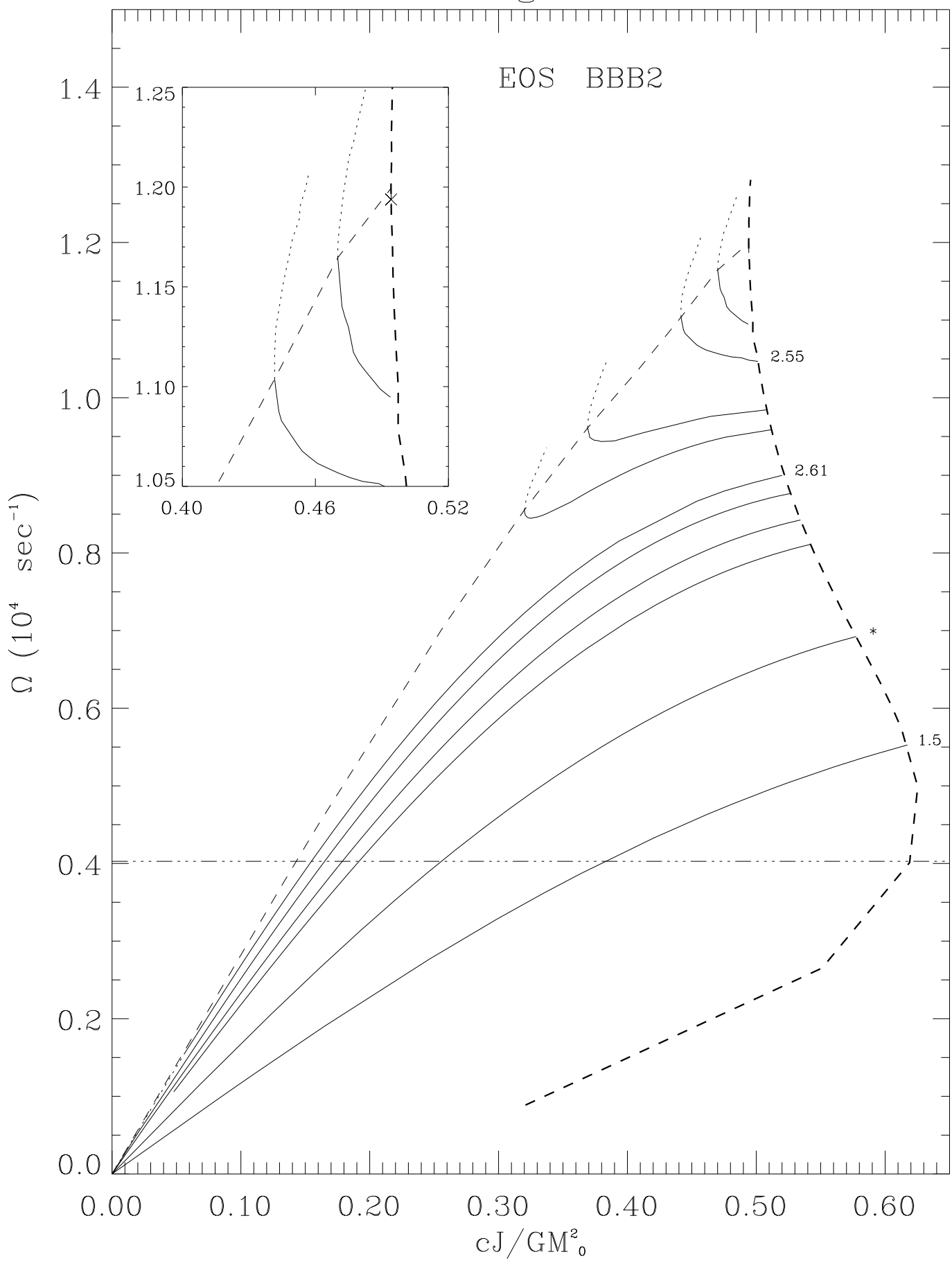


TABLE CAPTIONS

TABLE 1: Saturation properties for the various equations of state used in the present work: $n_o[fm^{-3}]$ is the saturation number density, $E_o/A[MeV/fm^3]$ the corresponding energy per nucleon and $K_o[MeV]$ the incompressibility of symmetric nuclear matter. $E_{sym}(n_o)[MeV]$ is the symmetry energy at the saturation point. In the last row we report the empirical saturation properties of nuclear matter.

TABLE 2: Maximum mass non-rotating models: the listed quantities are EOS models, central density (ϵ_c) in units of $g\ cm^{-3}$, gravitational mass (M_G) in solar units, radius (R) in km , baryonic mass (M_0) and proper mass (M_P) in solar units and lastly the radius (r_{orb}) of the innermost stable orbit in km . Note: the numbers following the letter E in column 2 of this and the subsequent tables, stand for powers of ten.

TABLE 3: Maximum mass rotating models: the listed quantities are EOS models, central density (ϵ_c) in units of $g\ cm^{-3}$, angular velocity (Ω) in units of $10^4\ rad\ s^{-1}$ of the neutron star as measured by an observer at infinity, moment of inertia (I) of neutron star in units of $10^{45}\ g\ cm^2$, gravitational mass (M_G) in solar units, ratio of the rotational energy to the total gravitational energy (T/W), radius (R) in km , eccentricity (e), ratio of inertial frame dragging at the center of the star to the rotation rate (ω_c/Ω_c), angular momentum (J) in 10^{49} cgs units, radius (r_{orb}) of the innermost stable orbit in km , the polar (Z_p), forward (Z_f) and backward (Z_b) redshifts, baryonic mass (M_0) and proper mass (M_P) in solar units.

TABLE 4: Maximum angular momentum models

TABLE 5: Constant Ω sequences: the sequences have angular velocity of the fastest known pulsar PSR 1937+21

FIGURE CAPTIONS

FIG 1: Speed of sound in beta-stable nuclear matter as a function of the nucleon number density for different models of EOS used in the present work. The three continuous lines refer from top to bottom of the figure to the BBB1, BPAL32 and BPAL21 model respectively; the dashed line is relative to the BBB2 EOS. The dot on each curve gives the speed of sound at the center of the non-rotating maximum mass configuration for that EOS model.

FIG 2: Pressure as a function of density for the new EOS models. Curves 1–4 stand for BBB1, BBB2, BPAL21 and BPAL32 respectively. Also shown for comparison are the EOS models BPAL12 (Bombaci 1995) a very soft EOS (represented by BPAL12 in figure) and Sahu, Basu & Datta (1993) a very stiff EOS (represented by CSM in figure).

FIG 3: The functional dependence of the gravitational mass with central density for EOS model BBB1. In this and all subsequent figures, the bold solid curve represents the non-rotating or static limit, and the bold dashed curve the centrifugal mass shed limit. The long dashed curve is the constant- Ω sequence corresponding to the period $P = 1.558$ ms. The thin solid curves that are roughly horizontal are the constant rest mass evolutionary sequences. The evolutionary sequences above the maximum stable non-rotating mass configuration, are the supramassive evolutionary sequences and those that are below this limit, are the normal evolutionary sequences. The almost vertical thin dashed line is the limit for instability against quasi-radial modes. The supramassive evolutionary sequences beyond the quasi-radial mode instability limit are represented by

dotted lines. The numbers against some of the curves in this and all subsequent figures represent the baryonic mass for the corresponding sequence; the equilibrium sequence that has $1.4 M_{\odot}$ configuration at the static limit is represented by an asterisk against it.

FIG 4: Gravitational mass (M_G) in solar units versus equatorial radius (R) in km for EOS model BBB1.

FIG 5: Neutron star rotation rate (Ω) in units of 10^4 rad s^{-1} versus its specific angular momentum (cJ/GM_0^2) for EOS model BBB1. The inset shows a close up view of the region surrounding the instability limit to quasi-radial mode near the mass shed limit.

FIG 6: $M_G - \epsilon_c$ relationship for EOS models BBB2.

FIG 7: $M_G - R$ variation for BBB2.

FIG 8: $\Omega - cJ/GM_0^2$ variation for BBB2.

TABLE 1

EOS	interaction	n_o	E_o/A	K_o	$E_{sym}(n_o)$
BBB1	Av14+TBF	0.178	-16.46	253	32.5
BBB2	Paris+TBF	0.176	-16.01	281	32.9
BPAL21	Skyrme-like	0.160	-16.00	180	30.0
BPAL32	Skyrme-like	0.160	-16.00	240	30.0
emp.sat.prop.		0.17 ± 0.01	-16 ± 1	220 ± 30	30 ± 2

TABLE 2

EOS	ϵ_c	M_G	R	M_0	M_p	r_{orb}	I
	($g\ cm^{-3}$)	(M_\odot)	(km)	(M_\odot)	(M_\odot)	(km)	($g\ cm^2$)
BBB1	3.09E+15	1.788	9.646	2.082	2.356	15.845	1.428E+45
BBB2	3.12E+15	1.917	9.519	2.261	2.608	16.984	1.593E+45
BPAL21	3.51E+15	1.684	9.292	1.940	2.222	14.921	1.191E+45
BPAL32	2.67E+15	1.947	10.509	2.263	2.579	17.254	1.826E+45

TABLE 3

EOS	ϵ_c	Ω	I	M_G	T/W	R	e	ω_c/Ω_c	J	r_{orb}	Z_p	Z_f	Z_b	M_0	M_p
BBB1	2.56E+15	1.095	2.428	2.135	0.120	13.129	0.703	0.764	2.658	13.490	0.690	-0.330	1.975	2.471	2.734
BBB2	2.82E+15	1.203	2.539	2.272	0.123	12.519	0.687	0.825	3.055	13.550	0.849	-0.349	2.483	2.653	3.008
BPAL21	3.03E+15	1.115	1.904	1.966	0.105	12.604	0.697	0.764	2.123	12.674	0.641	-0.323	1.811	2.253	2.530
BPAL32	2.27E+15	1.001	3.005	2.300	0.113	14.276	0.699	0.771	3.008	14.611	0.679	-0.328	1.933	2.657	2.962

TABLE 4

EOS	ϵ_c	Ω	I	M_G	T/W	R	e	ω_c/Ω_c	J	r_{orb}	Z_p	Z_f	Z_b	M_0	M_p
BBB1	2.44E+15	1.079	2.465	2.133	0.120	13.264	0.706	0.756	2.660	13.558	0.677	-0.328	1.935	2.468	2.721
BBB2	2.82E+15	1.203	2.539	2.272	0.123	12.519	0.687	0.825	3.055	13.550	0.849	-0.349	2.483	2.653	3.008
BPAL21	2.91E+15	1.100	1.933	1.965	0.106	12.730	0.699	0.757	2.125	12.733	0.630	-0.321	1.779	2.252	2.519
BPAL32	2.14E+15	0.981	3.070	2.299	0.114	14.481	0.702	0.760	3.011	14.713	0.661	-0.326	1.881	2.655	2.944

TABLE 5

EOS	ϵ_c	Ω	I	M_G	T/W	R	ϵ	ω_c/Ω_c	J	r_{orb}	Z_p	Z_f	Z_b	M_0	M_p
BBB1	5.21E+14	0.403	0.370	0.511	0.057	16.199	0.766	0.192	1.490	0.000	0.078	-0.167	0.326	0.526	0.539
	6.00E+14	0.403	0.510	0.658	0.048	12.950	0.603	0.237	2.052	0.000	0.104	-0.103	0.315	0.686	0.704
	1.00E+15	0.403	1.195	1.279	0.028	11.697	0.425	0.430	4.815	0.000	0.236	0.005	0.478	1.405	1.467
	1.40E+15	0.403	1.522	1.590	0.021	11.201	0.361	0.546	6.130	12.478	0.334	0.078	0.607	1.799	1.914
	1.90E+15	0.403	1.619	1.749	0.016	10.678	0.321	0.632	6.520	13.695	0.413	0.141	0.708	2.015	2.189
	2.40E+15	0.403	1.587	1.805	0.014	10.248	0.297	0.686	6.391	14.188	0.463	0.185	0.769	2.096	2.319
	2.90E+15	0.403	1.517	1.818	0.012	9.900	0.280	0.722	6.109	14.356	0.498	0.216	0.807	2.117	2.380
	3.00E+15	0.403	1.501	1.819	0.012	9.839	0.278	0.729	6.047	14.369	0.503	0.221	0.813	2.117	2.388
	3.30E+15	0.403	1.455	1.815	0.011	9.666	0.270	0.744	5.858	14.378	0.517	0.235	0.827	2.112	2.404
	3.40E+15	0.403	1.439	1.814	0.011	9.613	0.268	0.750	5.796	14.374	0.521	0.239	0.831	2.110	2.408
BBB2	5.01E+14	0.403	0.396	0.525	0.059	16.359	0.768	0.194	1.596	0.000	0.080	-0.169	0.331	0.541	0.554
	6.00E+14	0.403	0.587	0.713	0.048	12.965	0.590	0.250	2.363	0.000	0.113	-0.097	0.327	0.746	0.767
	1.00E+15	0.403	1.232	1.292	0.029	11.833	0.429	0.431	4.964	0.000	0.236	0.002	0.481	1.416	1.482
	1.40E+15	0.403	1.576	1.626	0.021	11.236	0.358	0.558	6.346	12.738	0.344	0.084	0.622	1.842	1.967
	1.90E+15	0.403	1.733	1.838	0.015	10.604	0.309	0.665	6.978	14.386	0.453	0.169	0.764	2.134	2.341
	2.40E+15	0.403	1.732	1.920	0.013	10.122	0.281	0.730	6.976	15.095	0.529	0.230	0.859	2.254	2.530
	2.90E+15	0.403	1.676	1.943	0.011	9.762	0.264	0.772	6.751	15.349	0.577	0.272	0.919	2.291	2.621
	3.10E+15	0.403	1.648	1.944	0.011	9.641	0.259	0.784	6.636	15.383	0.592	0.285	0.936	2.292	2.641
	3.30E+15	0.403	1.619	1.943	0.010	9.531	0.255	0.795	6.522	15.397	0.604	0.296	0.950	2.291	2.656
	3.40E+15	0.403	1.605	1.942	0.010	9.480	0.253	0.800	6.464	15.398	0.610	0.301	0.956	2.289	2.662

TABLE 5 (contd.)

EOS	ϵ_c	Ω	I	M_G	T/W	R	e	ω_c/Ω_c	J	r_{orb}	Z_p	Z_f	Z_b	M_0	M_p
BPAL21	5.19E+14	0.403	0.593	0.646	0.063	17.528	0.767	0.221	2.388	0.000	0.094	-0.178	0.368	0.671	0.687
	6.00E+14	0.403	0.698	0.758	0.053	14.288	0.631	0.256	2.812	0.000	0.113	-0.118	0.348	0.793	0.815
	1.50E+15	0.403	1.336	1.487	0.021	11.290	0.370	0.528	5.382	11.750	0.300	0.054	0.560	1.663	1.775
	2.05E+15	0.403	1.382	1.632	0.016	10.582	0.324	0.616	5.565	12.854	0.375	0.119	0.650	1.858	2.027
	2.50E+15	0.403	1.353	1.683	0.013	10.139	0.300	0.666	5.447	13.297	0.420	0.158	0.702	1.930	2.141
	2.95E+15	0.403	1.302	1.705	0.012	9.779	0.282	0.702	5.245	13.513	0.454	0.190	0.740	1.961	2.208
	3.80E+15	0.403	1.197	1.706	0.010	9.258	0.260	0.751	4.820	13.611	0.498	0.233	0.786	1.964	2.268
	4.65E+15	0.403	1.100	1.687	0.008	8.874	0.247	0.784	4.431	13.528	0.525	0.262	0.812	1.936	2.284
	5.55E+15	0.403	1.013	1.660	0.007	8.562	0.238	0.809	4.082	13.368	0.544	0.283	0.827	1.895	2.279
	5.95E+15	0.403	0.974	1.643	0.007	8.438	0.234	0.818	3.925	13.267	0.549	0.290	0.830	1.870	2.266
BPAL32	4.21E+14	0.403	0.903	0.764	0.076	18.581	0.776	0.234	3.639	0.000	0.106	-0.187	0.403	0.797	0.814
	6.00E+14	0.403	1.364	1.120	0.051	14.448	0.572	0.333	5.493	0.000	0.167	-0.088	0.430	1.198	1.234
	1.00E+15	0.403	1.959	1.621	0.031	13.062	0.434	0.494	7.888	0.000	0.284	0.008	0.577	1.808	1.904
	1.40E+15	0.403	2.124	1.848	0.022	12.239	0.371	0.595	8.554	14.331	0.370	0.078	0.686	2.108	2.268
	1.90E+15	0.403	2.086	1.955	0.017	11.488	0.329	0.673	8.401	15.191	0.443	0.141	0.775	2.261	2.493
	2.30E+15	0.403	1.996	1.982	0.015	11.032	0.306	0.715	8.037	15.463	0.483	0.177	0.821	2.300	2.582
	2.70E+15	0.403	1.895	1.984	0.013	10.664	0.290	0.746	7.631	15.548	0.512	0.205	0.853	2.305	2.627
	3.00E+15	0.403	1.821	1.977	0.012	10.433	0.281	0.765	7.333	15.544	0.529	0.221	0.870	2.295	2.645
	3.50E+15	0.403	1.706	1.958	0.011	10.109	0.270	0.789	6.872	15.462	0.549	0.243	0.889	2.267	2.656
	4.40E+15	0.403	1.533	1.915	0.009	9.665	0.256	0.820	6.176	15.218	0.572	0.270	0.906	2.202	2.645